Optimized Channel Phase Estimation in Passive RF Tag Network

Yang Xie*, Yang Li*, Petar M. Djurić*, Samir R. Das[†], and Milutin Stanaćević*
*Department of Electrical and Computer Engineering, Stony Brook University, Stony Brook, NY 11794

†Department of Computer Science, Stony Brook University, Stony Brook, NY 11794

Email: milutin.stanacevic@stonybrook.edu

Abstract—We present a method for passive wireless channel estimation in RF tag-to-tag link. The technique has a low computational complexity, a small memory footprint and requires only one additional port in the modulator design of RF tag. The performance of the proposed method is evaluated on distance estimation task. The performance in the range of tag-to-tag distance from 28 cm to 228 cm is limited to 10° (9 mm). The demonstrated performance is comparable to performance of distance estimation techniques based on RFID technology which utilize RFID reader and are not scalable as the proposed method. The proposed method is amenable to deployment in near zero power operation RF-powered tags and it enriches RF tags with the ability to passively 'fingerprint' their surrounding.

Index Terms—Backscatter, RFID, channel estimation, phase estimation, localization, low-power communication

I. INTRODUCTION

Wireless channel estimation, in addition to enhancing the communication link performance, has been widely used as a sensing modality due to unobtrusiveness of the approach [1]. Ability to remotely sense activities and interactions among various entities in the environment, is perceived to drive the future of Internet-of-Things (IoT) [2]. Human-centric applications range from human presence detection [3], [4], activity and/or gesture recognition [5]-[7], breathing/respiration and heart rate estimation [8], [9]. The main advantages of this sensing modality is that the human user does not have to wear device on the body while at the same time it preserves privacy of the user. WiFi sensing techniques rely on complex and computationally demanding signal processing and algorithms [10], while ultra-wideband (UWB) sensing requires generation of a complex environment scanning signal [11], [12]. A different approach has been focused on the techniques based on RFID technology, which mostly suffer from the high deployment cost [13], [14].

The required power consumption for wireless channel estimation in most of the applications where the receiver is integrated on a battery-less sensor node is prohibitively high. The wireless channel estimation technique for the passive RF tag-to-tag channel, with receiver based on envelope detector, has been introduced [15], [16]. The technique is based on the multi-phase modulator and demodulator that can measure the incident power at the receiving tag. The technique has been demonstrated in human activity recognition [17] and structural health monitoring [18]. The network of such RF tags, with ability for tag-to-tag channel estimation, naturally leads to a

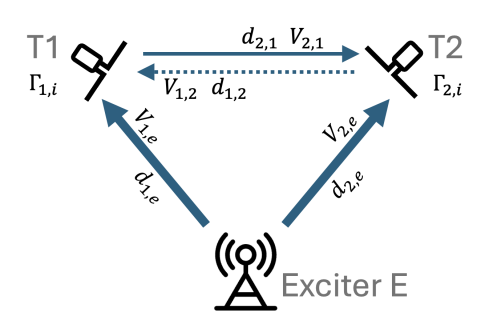


Fig. 1: Exciter E with two passive tags T_1 and T_2

vast number of RF links in a physical space providing a much richer granularity and redundancy for activity recognition and environmental/structural monitoring.

As RF tags operate on harvested RF energy, the computational load and the memory requirements are key performance parameters in determining their sensitivity and the operational range. We investigate technique that can significantly reduces both computation load and memory access and demonstrate the sustained performance in the distance estimation task.

The paper is organized as following. In Section II, we present a physical model of RF tag-to-tag link. The proposed method, based on the set of non-linear equations, is outlined in Section III. The performance of the method on synthetically generated and experimental data is shown and compared to the method based on the linearization of the derived channel model in Section IV. The concluding discussion is included in Section V.

II. BACKSCATTER CHANNEL MODELING

A backscatter-based tag-to-tag link, consisting of an exciter E and two passive transceiver tags T_1 and T_2 , is shown in Fig. 1. During the communication and channel sensing, one tag serves as the transmitter (Tx), scattering the incident wave from exciter, while the other tag operates in receiving mode (Rx), sensing a backscattered signal from the Tx tag superimposed on the excitation signal. According to antenna scattering theory, antennas exhibit two distinct modes of scattering incident energy: structural mode scattering, dependent on antenna structure, and antenna mode scattering, determined by the load impedance [19]. By manipulating the antenna load impedance, the amplitude and phase of the reflected incident

wave are modified, enabling the scattering tag to modulate and transmit information.

When tag T_1 is not reflecting, tag T_2 receives the signal from the exciter:

$$v_{2,e}(t) = A_{2,e}\cos(\omega t + \theta_{2,e}),$$
 (1)

where $A_{2,e}$ represents the amplitude of the received signal when the impedance of the demodulator of tag T_2 matches the impedance of its antenna, while $\theta_{2,e}$ signifies the channel phase from exciter to tag T_2 . $\omega = 2\pi f$ and f is the carrier frequency. According to Friis's equation the amplitude is given by:

$$A_{2,e} = \sqrt{P_e G_e G_2} \frac{\lambda}{4\pi d_{2,e}},$$
 (2)

where P_e is the transmit power of the exciter, G_e and G_2 are the antenna gains of the exciter and tag, respectively, λ is the wave length of the carrier frequency, and $d_{2,e}$ is the distance from the exciter to tag. Similarly, the incident voltage signal at tag T_1 is defined as:

$$v_{1,e}(t) = A_{1,e}\cos(\omega t + \theta_{1,e}),$$
 (3)

where $A_{1,e}$ is the amplitude of the received signal similar as $A_{2,e}$, and $\theta_{1,e}$ is the channel phase from the exciter to tag T_1 . When tag T_1 reflects the incident power from the exciter, T_2 receives the scattered signal from T_1 :

$$v_{2,1}(t) = \alpha_{2,1}|1 - \Gamma_1|A_{1,e}\cos(\omega t + \theta_{1,e} + \angle(1 - \Gamma_1) + \theta_{2,1}).$$

Here, Γ_1 is the reflection coefficient of tag T_1 , $|1 - \Gamma_1|$ is the backscattering coefficient determining the amount of coupled energy scattered [19]. $\alpha_{2,1}$ is the attenuation of the backscatter channel between tags T_1 to T_2 , and $\theta_{2,1}$ is the phase of the channel:

$$\alpha_{2,1} = \sqrt{G_1 G_2} \frac{\lambda}{4\pi d_{2,1}},\tag{5}$$

$$\theta_{2,1} = 2\pi \frac{d_{2,1}}{\lambda},\tag{6}$$

where $d_{2,1}$ is the distance between the tags. The demodulator of the passive tag is realized as an envelope detector that is designed to be conjugate matched to the antenna. Consequently, When tag T_2 is in receiving mode, the antenna mode scattering is zero, however its structural mode scattering still exists. The structural mode scattering results in a signal being initially reflected towards T_1 , subsequently redirected back, and ultimately received by T_2 . In (4), the structural mode scattering from receiving tag is not considered due to the long distance that this signal travels and therefore experiences high attenuation. From our experiments, we observed that such scattering may affect the accuracy of the channel phase estimation only when the tag-to-tag distance is less than the λ .

The received signal at tag T_2 is a superposition of the excitation signal $v_{2,e}(t)$ and backscatter signal $v_{2,1}(t)$. The amplitude of the combined signal, V_2 , can be expressed as:

$$V_{2}^{2} = A_{2,e}^{2} + \alpha_{2,1}^{2} |1 - \Gamma_{1}|^{2} A_{1,e}^{2}$$

$$+ 2A_{2,e}\alpha_{2,1} |1 - \Gamma_{1}| A_{1,e} \cos(\theta_{e,12} + \angle(1 - \Gamma_{1}))$$

$$= A_{2,e}^{2} + \alpha_{2,1}^{2} |1 - \Gamma_{1}|^{2} A_{1,e}^{2}$$

$$+ 2A_{2,e}\alpha_{2,1} A_{1,e} \cos(\theta_{2,e1})$$

$$+ 2A_{2,e}\alpha_{2,1} |\Gamma_{1}| A_{1,e} \cos(\theta_{2,e1} + \phi_{1})$$

$$(7)$$

where

$$\theta_{2,e1} = \theta_{1,e} + \theta_{2,1} - \theta_{2,e}. \tag{8}$$

and ϕ_1 is the phase of the reflection coefficient Γ_1 .

When tag T_2 backscatters, the amplitude of the combined received signal can be expressed in similar fashion as:

$$V_1^2 = A_{1,e}^2 + \alpha_{1,2}^2 |1 - \Gamma_2|^2 A_{2,e}^2$$

$$+2A_{1,e}\alpha_{1,2}A_{2,e}\cos(\theta_{1,e2})$$

$$+2A_{1,e}\alpha_{1,2}|\Gamma_2|A_{2,e}\cos(\theta_{1,e2} + \phi_2),$$
 (9)

where

$$\theta_{1,e2} = \theta_{2,e} + \theta_{1,2} - \theta_{1,e}. \tag{10}$$

and $|\Gamma_2|$ and ϕ_2 are the magnitude and phase of the reflection coefficient of tag T_2 , respectively. Due to the channel symmetry, $\alpha_{1,2}=\alpha_{2,1}$ and $\theta_{1,2}=\theta_{2,1}$.

III. CHANNEL PHASE ESTIMATION ALGORITHMS

The passive wireless sensing relies on estimating the tagto-tag channel phase, $\theta_{1,2}$, which is related to $\theta_{2,e1}$ and $\theta_{1,e2}$ as:

$$\hat{\theta}_{1,2} = \frac{\hat{\theta}_{2,e1} + \hat{\theta}_{1,e2}}{2} \mod \pi \tag{11}$$

To estimate $\theta_{2,e1}$, we obtain a set of equations in the form of (7) by recording the voltage $V_{2,i}$ at tag T_2 for a set of N reflection coefficients $\Gamma_{1,i}$ at the tag T_1 , where i=0 to N-1. We denote the amplitude $V_{2,0}$ as the amplitude for which the tag T_1 is terminated with the complex conjugate matching with the antenna impedance. For the reflection coefficients $\Gamma_{1,i}$, i=1 to N-1, to maximize the signal-to-noise ratio, we select the magnitude of all reflection coefficients close to unity, with the phases, $\phi_{1,i}$ uniformly spanning the range from $-\pi$ to π . To estimate $\theta_{2,e1}$ from this set of N non-linear equations, we present two approaches and then compare their accuracy and computational efficiency for phase estimation task.

The phase-based estimation of distance suffers from an ambiguity due to the phase wraparound. As we are estimating $\theta \pmod{\pi}$, the tag-to-tag distance $d_{1,2}$ is

$$d_{1,2} = \frac{\lambda}{2\pi}\hat{\theta} + k\frac{\lambda}{2}.\tag{12}$$

The unknown k causes the ambiguity in distance estimation. To overcome this ambiguity, a fingerprinting method [15] has been proposed.

A. Technique based on linear least squares(LLS)

Implementing the phase estimation algorithm on a passive tag relying on harvested energy demands meticulous attention to both computational complexity and accuracy. The set of N non-linear equations can be transformed into a set of N linear equation by using the following approximations [15]:

$$\alpha_{2,1}|1 - \Gamma_1|A_{1,e} \ll 2A_{2,e}\cos(\theta_{e,12} + \angle(1 - \Gamma_1))$$
 (13)

$$2\alpha_{2,1}|1-\Gamma_1|\frac{A_{1,e}}{A_{2,e}}\cos(\theta_{e,12}+\angle(1-\Gamma_1))\ll 1.$$
 (14)

The approximations are based on $\alpha_{2,1} \ll 1$ and similar order of excitation power at both tags. Using these approximations, (7) simplifies to:

$$V_{2,i} = A_{2,e} + A_{1,e}\alpha_{2,1}[(1 - |\Gamma_{1,i}|\cos\phi_{1,i})\cos\theta_{2,e1} + |\Gamma_{1,i}|\sin\phi_{1,i}\sin\theta_{2,e1}].$$
(15)

This equation can be expanded into a matrix representation $V_2 = H_1 x_1$ as equation 16.

$$\underbrace{\begin{bmatrix} V_{2,0}...V_{2,N-1} \end{bmatrix}}_{v_2} = \underbrace{\begin{bmatrix} 1 & 1 - |\Gamma_{1,1}|\cos\phi_{1,0} & |\Gamma_{1,1}|\sin\phi_{1,1} \\ ... & ... & ... \\ 1 & 1 - |\Gamma_{1,8}|\cos\phi_{1,N-1} & |\Gamma_{1,N}|\sin\phi_{1,N-1} \end{bmatrix}}_{H_1} \\
\underbrace{\begin{bmatrix} A_{2,e} \\ A_{1,e}\alpha_{2,1}\cos\theta_{2,e1} \\ A_{1,e}\alpha_{2,1}\sin\theta_{2,e1} \end{bmatrix}}_{T_1} \tag{16}$$

 H_1 is a known Nx3 matrix, so we can use linear least squares solution to obtain estimate of x_1 as

$$\hat{x}_1 = (H_1^T H_1)^{-1} H_1^T v_2. (17)$$

Estimate of $\theta_{2,e1}$ can be obtained as

$$\hat{\theta}_{2,e1} = \operatorname{atan} \frac{\hat{x}_1(3)}{\hat{x}_1(2)}.$$
 (18)

B. Technique with optimized set of three modulation loads

The cost of tags presents a significant challenge to largescale deployment, while ensuring low power consumption is of fundamental importance. Therefore, simplifying the circuitry of tags is crucial to reduce both costs and energy usage. Employing RF-switch with fewer ports would be a favorable proposition. We propose an approach that utilizes a set of two non-linear equations (3) without linearizing the model.

From (16), channel phase estimation can be performed with three reflection loads. The challenge lies in selecting the reflection coefficients that offer the most accurate estimate of the channel phase. To tackle this challenge, we propose an technique that leverages the reflection coefficients of two modulators and the demodulator(i = 0). Since $|\Gamma_0| \approx 0$ and $|1 - \Gamma_0|^2 \approx 1$, from (7), the difference between the voltage

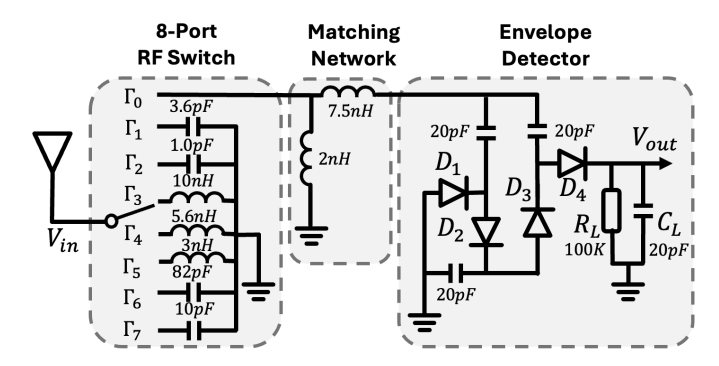


Fig. 2: Schematic of the designed backscatter RF tag

amplitude at tag T_2 contributed by the reflection coefficient $\Gamma_{1,i}$ and $\Gamma_{1,0}$ of tag T_1 , is:

$$V_{2,i}^2 - V_{2,0}^2 = (|1 - \Gamma_{1,i}|^2 - 1)\alpha_{2,1}^2 A_{1,e}^2 + 2|\Gamma_{1,i}|A_{2,e}\alpha_{2,1}A_{1,e}\cos(\theta_{2,e1} + \phi_{1,i})$$
(19)

By selecting the $\Gamma_{1,0}$ as the reference signal, we observe that the optimal selection of the two reflection coefficients should eliminate the first term in (19),

$$w_i = |1 - \Gamma_{1,i}|^2 - 1. (20)$$

If we select the two reflection coefficients, $\Gamma_{1,a}$ and $\Gamma_{1,b}$ that satisfy the above condition, we observe the following ratio

$$\gamma = \frac{V_{2,a}^2 - V_{2,0}^2}{V_{2,b}^2 - V_{2,0}^2} \frac{2|\Gamma_{1,b}|}{2|\Gamma_{1,a}|} = \frac{\cos(\theta_{2,e1} + \phi_{1,a})}{\cos(\theta_{2,e1} + \phi_{1,b})}$$
(21)

and then estimate the channel phase from measure γ and known $\phi_{1,a}$ and $\phi_{1,b}$ as

$$\hat{\theta}_{2,e1} = \tan \frac{\gamma \cos \phi_{1,b} - \cos \phi_{1,a}}{\gamma \sin \phi_{1,b} - \sin \phi_{1,a}}$$
(22)

In this approach, the accuracy is determined by value of w_i and selection of $|\Gamma_{1,a}|$ and $|\Gamma_{1,b}|$ that lead to minimal w_a and w_b . Additionally, the magnitude $|\Gamma_{1,a}|$ and $|\Gamma_{1,b}|$ should be maximazed to increase the signal-to-noise ratio in measured γ . If we assume that the magnitude of $|\Gamma|$ is unity, two phases of $|\Gamma|$ result in w=0, $\phi_{1,a}=-60^\circ$ and $\phi_{1,b}=60^\circ$.

IV. RESULTS

In section III, two different channel phase estimation approaches are presented. In this section, we describe the implementation of the tag using discrete components. To evaluate the accuracy of the presented phase estimation algorithms, we first generate data based on the backscatter channel model by applying the eight reflection coefficients of the fabricated tag to this model and compare the performance of the algorithms for phase estimation. Lastly, we present the experimental setup and quantify the performance of the estimation algorithms.

A. Tag Implementation

We have implemented a discrete prototype of the backscatter RF tag. Fig. 2 and 3 depict the schematic and PCB implementation, including a multi-port modulator and demodulator. An 8-port reflective RF switch (Skyworks Sky13418) connects

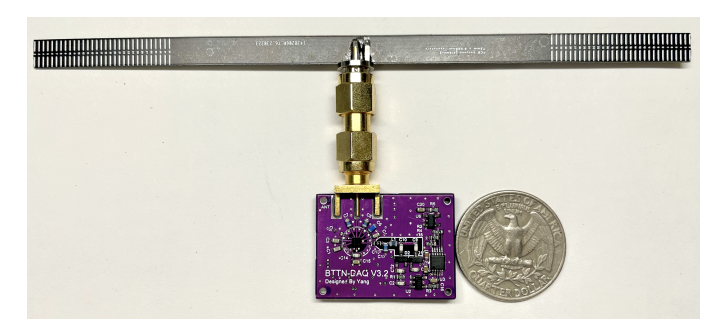


Fig. 3: Prototype of the backscatter RF tag.

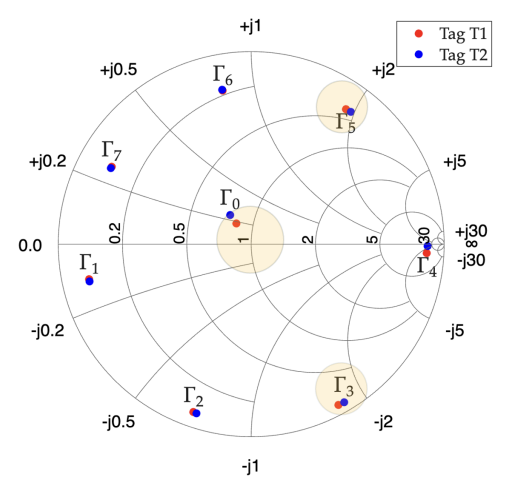


Fig. 4: Γ on the Smith chart, each with 50° gap except Γ_0

to a half-wave PCB dipole antenna. Seven out of the eight ports are connected to distinct impedance loads, Γ_1 to Γ_7 , with a 50-degree phase gap, constituting the modulator. The remaining port, connected to a reverse L matching network which is conjugate matched to 50 Ω at 915 MHz with its antenna, represented as Γ_0 , serves as the receiving path for the demodulator. The impedance of all the eight channels under input power -25 dBm at 915 MHz are shown in Fig. 4.In the demodulator, following the matching network, a two-stage voltage multiplier is employed for envelope extraction. This multiplier utilizes the zero bias Schottky diode pair SMS7630-006LF from Skyworks. The envelope detector is succeeded by a high-resolution 16-bit 1 Mbps ADC (TI ADS8860) with a 2.5 V reference voltage.

B. Simulation Results

A setup depicted in Fig. 5 was utilized to emulate a distance estimation experiment. Tag T_1 remained stationary at a distance of 302 cm from the exciter, while tag T_2 was positioned at various tag-to-tag distances ranging from 28 cm to 228 cm away from T_1 . At a distance of 228 cm, tag T_2 , along with tag T_1 and the exciter, geometrically forming an isosceles triangle. The setup was arranged within an area of 4.6 m by 4.6 m, aiming to simulate indoor sensing applications.

The initial step of the simulation involves emulating input voltage at the receiving tag, when modulator is in reflection

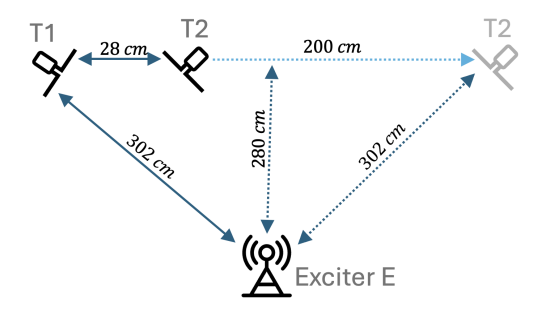


Fig. 5: Experimental setup for synthetic data generation for quantifying the performance of phase estimation.

state i. The input signal $V_{2,i}$ is derived from the superposition of (3) and (4), and is expressed as

$$V_{2,i} = \left| \frac{\lambda \sqrt{P_e G_e G_2 R_0}}{4\pi d_{2,e} \sqrt{2}} e^{-j(\frac{2\pi f d_{2,e}}{c})} + \frac{|1 - \Gamma_{1,i}| \lambda^2 G_1 \sqrt{P_e G_e G_2 R_0}}{16\pi^2 d_{1,e} d_{2,1} \sqrt{2}} e^{-j(\frac{2\pi f (d_{2,1} + d_{1,e})}{c} + \phi_{1,i})} \right|.$$
(23)

where R_0 represents 50 Ω and c is speed of light. G_e equals 8.5 dBi as the gain of the exciter antenna, G_1 and G_2 are 2.1 dBi as the gain of tag's dipole antenna. P_e is set as 13 dBm as the excitation power. $\Gamma_{1,i}$ and $\phi_{1,i}$ are the reflection coefficient and phase of the fabricated tag, while d is the tagto-tag distance. By applying these parameters into (23), the amplitude of the input signal to the envelope detector, $V_{1,i}$ and $V_{2,i}$, are acquired.

1) Performance of LLS method: The performance of the linear least squares (LLS) method is shown in Fig. 6. The scatter plot in the upper figure represents the phase estimation results, with the dashed line indicating its ideal value. The lower plot displays the estimation error in degrees. The mean absolute error (MAE) is 1.0° . For 915 MHz, with λ = 327.6 mm, the MAE of the distance estimation error translates to 0.9 mm.

The matrix H_i in (18) consists of known parameters of the tag and can be directly loaded into the tag. Estimating the phase requires only a few matrix operations. Thus, this method proves to be a feasible approach for implementation on passive tags, owing to its high accuracy and low computational requirement.

2) Performance of three-modulation loads method: We showed that assuming ideal unity of the magnitude of the reflection coefficient, optimal reflection phases are -60° and 60° . However, due to the resistive loss, the magnitude of the reflection coefficient is not unity. The colored region on the Smith chart 4 illustrates the accessible impedance on the implemented RF tag that can minimize w.

In Table I we present an exhaustive list of all possible pairs for selection of Γ_a and Γ_b out of seven loads implemented on the actual tag. We note the corresponding values of w_a and w_b alongside obtained respective estimation error with the synthetically generated data. Notably, the combination involving Γ_3 and Γ_5 , exhibiting S11 values of (-0.46 dB,

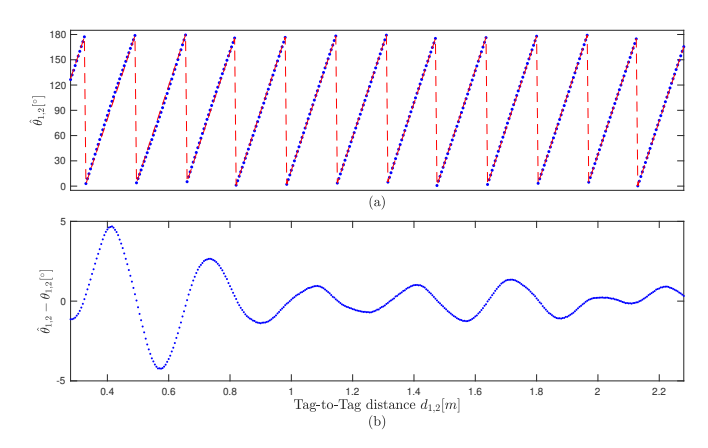


Fig. 6: Phase estimation results of the LLS method on synthetically generated data. (a) Estimated channel phase vs. ideal. (b) Phase estimation error.

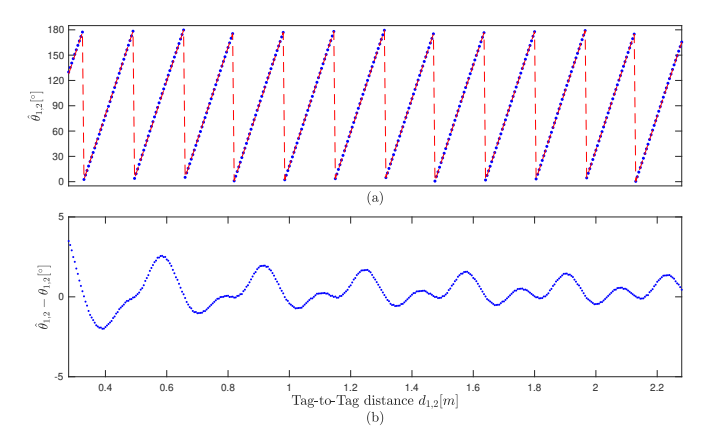


Fig. 7: Phase estimation results of the three-modulation loads method on synthetically generated data. (a) Estimated channel phase vs. ideal. (b) Phase estimation error.

 $-62^\circ)$ and $(-1.36~\text{dB},\,65^\circ)$ of the actual tag, demonstrates the lowest estimation error. This finding is consistent with the optimization methodology we have proposed. Fig. 7 shows comparable precision of the optimized three-modulation loads method to the LLS method involving seven phases.



Fig. 8: Experimental setup for quantifying the performance of the two methods.

TABLE I: Combinations of w_a , w_b and the corresponding estimation errors

a, b	w_a	w_b	stddev of errors [°]
1, 2	2.17	1.21	3.1
1, 3	2.17	-0.25	3.3
1, 4	2.17	-1.23	4.4
1, 5	2.17	-0.24	4.7
1, 6	2.17	0.71	3.7
1, 7	2.17	1.89	3.3
2, 3	1.21	-0.25	2.6
2, 4	1.21	-1.23	2.3
2, 5	1.21	-0.24	2.8
2, 6	1.21	0.71	9.3
2, 7	1.21	1.89	3.4
3, 4	-0.25	-1.23	1.6
3, 5	-0.25	-0.24	1.0
3, 6	-0.25	0.71	1.8
3, 7	-0.25	1.89	5.4
4, 5	-1.23	-0.24	1.7
4, 6	-1.23	0.71	2.4
4, 7	-1.23	1.89	4.9
5, 6	-0.24	0.71	2.6
5, 7	-0.24	1.89	3.1
6, 7	0.71	1.89	3.0

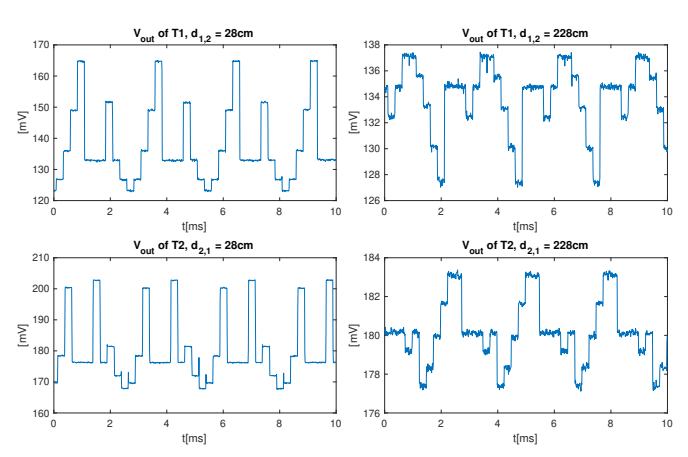


Fig. 9: Voltage outputs of the envelope detector for the MPP packets.

C. Experimental Results

To quantify and compare the performance of the two methods, we conducted experiments using a setup, depicted in Fig. 8, consistent with the simulation setup. The exciter transmits 13 dBm RF wave at 915 MHz with 8.5 dBi circularly polarized antenna. Both RF tags were equipped with a 2.15 dBi dipole antennae. During the experiments, the transmitting tag backscatters the received signal by altering its load impedance with a sequence $\{0, 0, 0, 1, 0, 2, 3, 4, 5, 6, 7\}$. This sequence, a multi-phase probing (MPP) packet, involved a transmitting interval of 250 μ s for each load, with a receiving ADC sampling frequency of 100 kHz. For each specified tag-to-tag distance, multiple MPP packets are dispatched, guaranteeing that high phase estimation precision is obtained in the presence of noise and interference. Fig. 9 illustrates the voltage outputs received by tags T_1 and T_2 at tag-to-tag distances of 28 cm and 228 cm, respectively, for the MPP packets.

Fig. 10 shows the estimated tag-to-tag channel phase $\hat{\theta}_{1,2}$

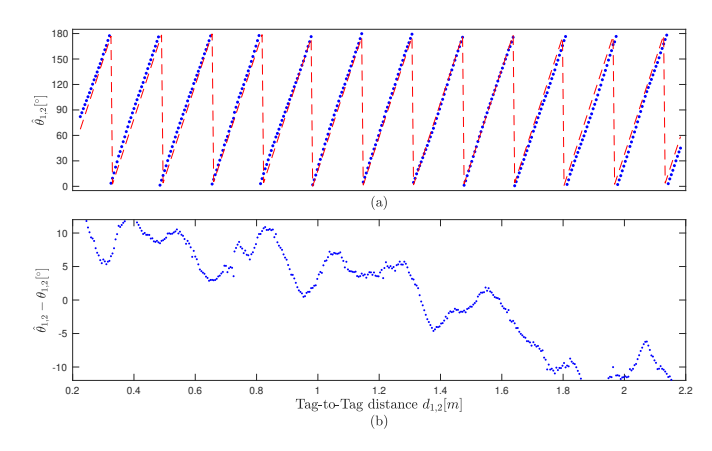


Fig. 10: Phase estimation results using the LLS method on experimental data. (a) Estimated channel phase vs. ideal. (b)

Phase estimation error.

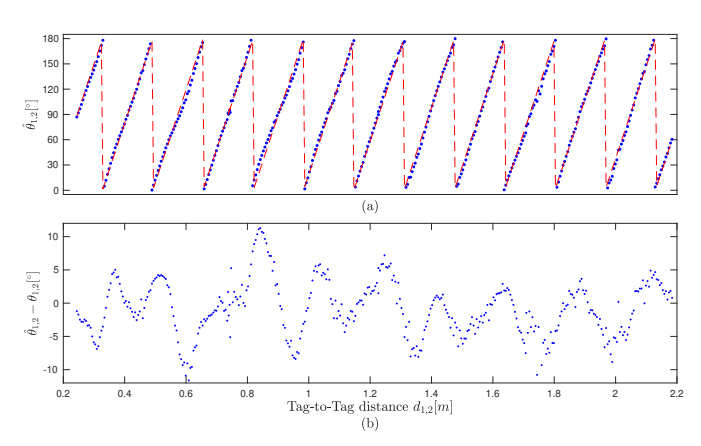


Fig. 11: Phase estimation results using the three-modulation loads method on experimental data. (a) Estimated channel phase vs. ideal. (b) Phase estimation error.

and the estimation error $\hat{\theta}_{1,2}$ - $\theta_{1,2}$, when we applied LLS method on the experimental data. Similarly, Fig. 11 shows the estimated channel phase and estimation error for optimized three-modulation loads method. Both methods demonstrate similar accuracy. The estimation error for the proposed three-modulation loads method is limited to 10° (9 mm).

V. CONCLUSIONS

We proposed a computationally light algorithm that estimates the tag-to-tag channel phase with only three modulation loads, one of which can be the demodulator, on the transmitting tag side. The performance of the proposed method has been quantified in both simulations and experiments, and compared with the method based on the linearization of the channel model. Future work will involve deploying a network of RF tags implementing the proposed method, and assessing the accuracy of localization.

ACKNOWLEDGEMENT

This work was supported by the National Science Foundation (NSF) under grants CNS-1901182 and CPS-2038801.

REFERENCES

- [1] Y. Ma, G. Zhou, and S. Wang, "Wifi sensing with channel state information: A survey," *ACM Computing Surveys (CSUR)*, vol. 52, no. 3, pp. 1–36, 2019.
- [2] U. S. Toro, K. Wu, and V. C. Leung, "Backscatter wireless communications and sensing in green internet of things," *IEEE Transactions on Green Communications and Networking*, vol. 6, no. 1, pp. 37–55, 2021.
- [3] F. Adib and D. Katabi, "See through walls with wifi!" in Proceedings of the ACM SIGCOMM 2013 conference on SIGCOMM, 2013, pp. 75–86.
- [4] T. Xin, B. Guo, Z. Wang, P. Wang, J. C. K. Lam, V. Li, and Z. Yu, "Freesense: A robust approach for indoor human detection using wi-fi signals," *Proceedings of the ACM on Interactive, Mobile, Wearable and Ubiquitous Technologies*, vol. 2, no. 3, pp. 1–23, 2018.
- [5] W. Wang, A. X. Liu, M. Shahzad, K. Ling, and S. Lu, "Device-free human activity recognition using commercial wifi devices," *IEEE Journal on Selected Areas in Communications*, vol. 35, no. 5, pp. 1118–1131, 2017.
- [6] Y. Zheng, Y. Zhang, K. Qian, G. Zhang, Y. Liu, C. Wu, and Z. Yang, "Zero-effort cross-domain gesture recognition with wi-fi," in *Proceedings of the 17th annual international conference on mobile systems*, applications, and services, 2019, pp. 313–325.
- [7] S. Palipana, D. Rojas, P. Agrawal, and D. Pesch, "Falldefi: Ubiquitous fall detection using commodity wi-fi devices," *Proceedings of the ACM on Interactive, Mobile, Wearable and Ubiquitous Technologies*, vol. 1, no. 4, pp. 1–25, 2018.
- [8] S. Yue, H. He, H. Wang, H. Rahul, and D. Katabi, "Extracting multiperson respiration from entangled rf signals," *Proceedings of the ACM on Interactive, Mobile, Wearable and Ubiquitous Technologies*, vol. 2, no. 2, pp. 1–22, 2018.
- [9] Y. Zeng, D. Wu, J. Xiong, J. Liu, Z. Liu, and D. Zhang, "Multisense: Enabling multi-person respiration sensing with commodity wifi," Proceedings of the ACM on Interactive, Mobile, Wearable and Ubiquitous Technologies, vol. 4, no. 3, pp. 1–29, 2020.
- [10] D. Vasisht, S. Kumar, and D. Katabi, "{Decimeter-Level} localization with a single {WiFi} access point," in 13th USENIX symposium on networked systems design and implementation (NSDI 16), 2016, pp. 165–178.
- [11] F. Zhang, Z. Chang, J. Xiong, J. Ma, J. Ni, W. Zhang, B. Jin, and D. Zhang, "Embracing consumer-level uwb-equipped devices for finegrained wireless sensing," *Proceedings of the ACM on Interactive, Mobile, Wearable and Ubiquitous Technologies*, vol. 6, no. 4, pp. 1– 27, 2023.
- [12] F. Adib, Z. Kabelac, D. Katabi, and R. C. Miller, "3d tracking via body radio reflections," in 11th USENIX Symposium on Networked Systems Design and Implementation (NSDI 14), 2014, pp. 317–329.
- [13] F. Costa, S. Genovesi, M. Borgese, A. Michel, F. A. Dicandia, and G. Manara, "A review of rfid sensors, the new frontier of internet of things," *Sensors*, vol. 21, no. 9, p. 3138, 2021.
- [14] J. Liu, X. Chen, S. Chen, X. Liu, Y. Wang, and L. Chen, "Tagsheet: Sleeping posture recognition with an unobtrusive passive tag matrix," in IEEE INFOCOM 2019-IEEE Conference on Computer Communications. IEEE, 2019, pp. 874–882.
- [15] A. Ahmad, X. Sha, M. Stanaćević, A. Athalye, P. M. Djurić, and S. R. Das, "Enabling passive backscatter tag localization without active receivers," in *Proceedings of the 19th ACM Conference on Embedded Networked Sensor Systems*, 2021, pp. 178–191.
- [16] A. Ahmad, X. Sha, A. Athalye, S. Das, P. Djurić, and M. Stanaćević, "Amplitude and phase estimation of backscatter tag-to-tag channel," in 2022 IEEE International Symposium on Circuits and Systems (ISCAS). IEEE, 2022, pp. 1342–1346.
- [17] J. Ryoo, Y. Karimi, A. Athalye, M. Stanaćević, S. R. Das, and P. Djurić, "Barnet: Towards activity recognition using passive backscattering tagto-tag network," in *Proceedings of the 16th annual international confer*ence on mobile systems, applications, and services, 2018, pp. 414–427.
- [18] A. Ahmad, X. Sha, A. Athalye, S. R. Das, K. Caylor, B. Glisic, M. Stanacevic, and P. M. Djuric, "Dispersed passive rf-sensing for 3d structural health monitoring," *ITU Journal on Future and Evolving Technologies*, vol. 3, no. 2, 2022.
- [19] F. Fuschini, C. Piersanti, F. Paolazzi, and G. Falciasecca, "Analytical approach to the backscattering from UHF RFID transponder," *IEEE Antennas and Wireless Propagation Letters*, vol. 7, pp. 33–35, 2008.